Study of Photovoltaic Parameters of Efficient Bulk-Heterojunction Organic Solar Cells for Indoor Applications Under Varied Intensities and Indoor LED Lighting

Shyam Shankar S, Kanupriya Khandelwal, Gaurav Gupta, and Ganesh D. Sharma

***Abstract*—Bulk-heterojunction devices with D18 and Y12 as active material were fabricated with an inverted ITO/zinc oxide/active material/molybdenum (III) oxide/Ag structure. Donor D18 and acceptor Y12 have complementary absorption spectra covering the visible range (300–800 nm). Furthermore, the energy layer alignment of these materials also makes it easier for charge generation and transport. All these factors lead to exploiting the possibility of using these organic solar cells (OSCs) for indoor photovoltaic (IPV) applications. The devices prepared previously were soaked in light (AM1.5 G) and illuminated under three types of white LED: warm white, standard white, and cool white. The intensities of the lights were varied, and the photovoltaic parameters of the cells were recorded. The variation of photovoltaic parameters with the intensity and color-correlated temperature (CCT) of different lights was thoroughly studied in this work. The external quantum efficiency of devices was also recorded. Here, we obtained cells with a power conversion efficiency (PCE) of 12.88% in AM1.5 G, which went up to 27.58% in indoor lighting. All the devices were prepared without the nitrogen glovebox and were characterized in ambient conditions, which is the first step toward commercializing and integrating the cells in the Internet of Things (IoTs). IPV, being an emerging field, the study of photovoltaic parameters under varied intensity of light and different lights reveals a lot of information about the behavior of cells. Such a study has never been performed before, and the correlation between intensity and CCT of light with photovoltaic parameters and PCE unveils invaluable information about indoor OSCs. The results of this study could potentially aid in optimizing and developing OSC for self-sustaining IoTs in the near future.**

***Index Terms*—Indoor photovoltaics (IPVs), Internet of Things (IoTs), organic solar cells (OSCs), power conversion efficiency (PCE).**

I. Introduction

SOLAR energy is the ultimate winner in man's search for greener, cleaner, cheaper, and more available sources for energy production. In order to convert solar energy into electrical energy, among all solar cells, organic solar cells (OSCs) have gained significant interest due to their inherent benefits, such as flexibility, low weight, and semitransparency [1], [2], [3], [4]. With the emergence of nonfullerene acceptors (NFAs), the efficiency of OSCs has seen remarkable progress, with the power conversion efficiency (PCE) reaching up to 20% [5], [6], [7], [8], [9], [10], [11]. In recent years, there has been very rapid growth in the development of the Internet of Things (IoTs). Wireless sensors, low-power wireless headsets, and other small electronic gadgets rule the industry. One of the striking features of these IoTs is that they require meagre power (usually in the range of 1–100 μW) for their work. When illuminated by indoor lighting, OSCs pose a better alternative for powering up these devices [12], [13], [14], [15], [16], [17], [18]. White LED lights, which are standard in rooms, offices, or any other indoor setting, are sufficient to power up the IoTs. The spectral properties of OSC can be modified easily and show a high correlation with the indoor light spectra [19], [20]. With the advent of NFAs, indoor OSC efficiencies have reached the range of 30%–33% under LED illumination, which is still much less than the Shockley–Queisser limit for indoor photovoltaic (IPV) applications [21], [22], [23], [24]. This suggests a massive impact OSC can create on the future of self-sufficient IoTs.

The performance of OSC under indoor lighting depends mainly on three parameters. First, the absorption spectra of the organic active layer must overlap with the emission spectra of the indoor lighting spectrum. Indoor lighting falls in the visible region (300–800 nm), making organic semiconducting materials a good contender. Second, the color-correlated temperature (CCT) light directly correlates to the spectral distribution, which helps decipher the organic semiconducting material that can yield maximum output. LEDs with higher CCT have more emission in the blue region. The choice of CCT is usually personal. Warm white (WW) LEDs are preferred in private spaces, such as bedrooms or living rooms as they have a calming effect. "Cool white (CW) LEDs" are traditionally kept in workspaces as they increase productivity [25]. Third, the intensity of the input light affects the device's photovoltaic parameters, determining the performance [26], [27], [28].

Received 6 June 2025; accepted 23 June 2025. Date of publication 13 August 2025; date of current version 23 October 2025. *(Corresponding author: Ganesh D. Sharma.)*

The authors are with the Department of Physics, The LNM Institute of Information Technology (Deemed University), Jaipur 302031, India (e-mail: ssk971996@gmail.com; 19pph004@lnmiit.ac.in; 18pph004@lnmiit.ac.in; gdsharma273@gmail.com).

This article has supplementary downloadable material available at https://doi.org/10.1109/JPHOTOV.2025.3592679, provided by the authors.

Digital Object Identifier 10.1109/JPHOTOV.2025.3592679

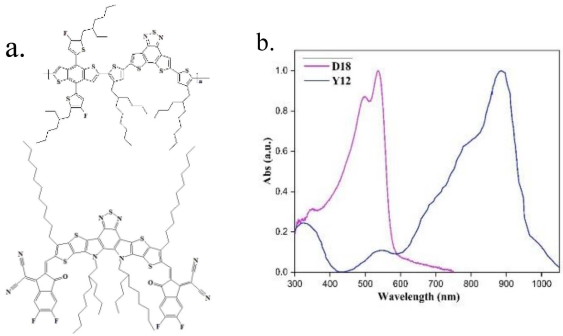

Fig. 1. (a) Chemical structure and (b) thin film absorption spectra of pristine D18 and Y12.

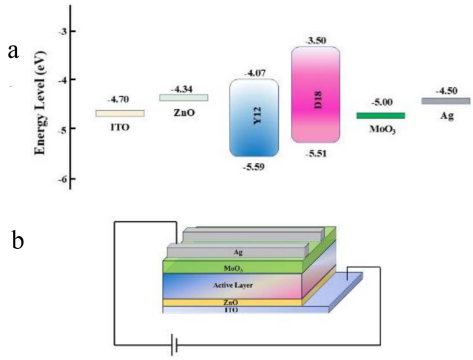

Fig. 2. (a) Energy level of different components of OSC. (b) Structure of the device.

Apart from the materials selection strategy mentioned above, the performance of OSC can be further improved or optimized by device architecture. Bulk-heterojunction (BHJ) devices are the most commonly used architecture in OSC, owing to better dissociation, collection, and transportation of excitons than bilayer or monolayer OSC. The donor and acceptor materials blend, leading to an increase in the interfacial area and charge separation. Proper electron transporting material (ETL) and hole transporting materials (HTL) are chosen to transport the dissociated electrons and holes to electrodes for photocurrent generation [2], [29], [30]. Most recent works in OSC focus on BHJ architecture and successful optimization of subsequent layers, morphology control of blend, and adapting various strategies to avoid recombination, which have yielded around 19% PCE under 1 sun [31].

In this work, the polymers D18 and Y12 were used as donors and NFAs, respectively, to make indoor OSC devices, and their chemical structures are shown in Fig. 1(a). D18 is an excellent copolymer with a fused ring acceptor unit, dithienobenzothiadiazole (DTBT). Including DTBT in the polymer results in a larger molecular plane and, thus, higher hole mobility [32]. The Y12 (BTP-4F-12) is derived from Y6 (BTP-4F). Being more soluble in greener solvents and also used as a low band gap polymer without any fullerene, Y12 is an excellent acceptor material. D18 and Y12 are blended into a solution to make BHJ OSCs of inverted architecture. Inverted architecture is preferred over the conventional structures as it shows more stability in the ambient atmosphere [33], which is vital for commercialization in the future. Devices are then illuminated under 1 sun (AM1.5 G), and their photovoltaic parameters are studied. The experiment focuses on the performance of the device under the illumination of a white LED, which is widely used in indoor settings, such as homes and offices. CCT of the white light is varied for WW, standard white (SW), and CW LEDs, as they are very common in households. All the photovoltaic parameters under these different lighting conditions are thoroughly focused and correlated. This work provides invaluable insights into the type of indoor lighting that could be better suited for IPV and sheds light on the mechanisms happening in the devices.

II. Results and Discussion

Indoor lighting covers only the visible spectrum (300–800 nm). Hence, we require material that absorbs light well in this particular region. We have chosen D18 as donor material and Y12 as acceptor material for the above-stipulated purpose. D18 and Y12 have complementary absorption spectra viable for donor–acceptor blends [see Fig. 1(b)]. The absorption spectra of D18 show a strong absorption from 400 to around 630 nm, as seen in Fig. 1(b). This covers the majority of the visible spectrum. Y12 offers absorption [see Fig. 1(b)] from 600 nm and extends to 800 nm [34]. The D18 and Y12 show complementary absorption covering the visible range (350–800 nm).

The highest occupied molecular orbital (HOMO) and lowest unoccupied molecular orbital (LUMO) of both materials are estimated using cyclic voltammetry (CV) [see Fig. S2(a) and (b) of the Supplementary Material]. The energy band diagram [see Fig. 2(a)] shows both the HOMO and LUMO levels of donor and acceptor materials, which shows their viability for the device fabrication. Zinc oxide (ZnO) was chosen as the ETL because of its excellent electron mobility and energy alignment [35]. Also, ZnO shows high transmittance, which makes it easier for photons to reach the active layer for exciton dissociation [36]. Molybdenum (III) oxide (MoO_3) is used as the HTL as it shows high hole mobility and proper energy alignment. Silver (Ag) is used as a cathode, owing to its high conductivity and alignment [37]. The energy band diagram [see Fig. 2(a)] depicts the energy levels of all the materials for the device [30].

The inverted structure of the OSC helps stabilize the device in the ambient environment [38]. All the steps in the device fabrication are done without using a glove box. Furthermore, all the characterization was done in standard atmospheric conditions. This ensures that the device performs well in room conditions as a part of the first step toward commercialization. The donor and acceptor of a particular ratio are taken and blended in a chlorobenzene solution. The detailed experimental procedure is discussed in the supplementary material. The device structure is ITO/ZnO/active layer/MoO_3/Ag [see Fig. 2(b)].

A. Photovoltaic Properties

The current–voltage (J–V) characterizations of the devices were done under 1 sun conditions (AM1.5 G) and are shown in Fig. 3(a), and photovoltaic parameters were calculated (see Table I). We can see that the device performs well due to proper energy-level alignment, achieving a PCE of 12.88% with

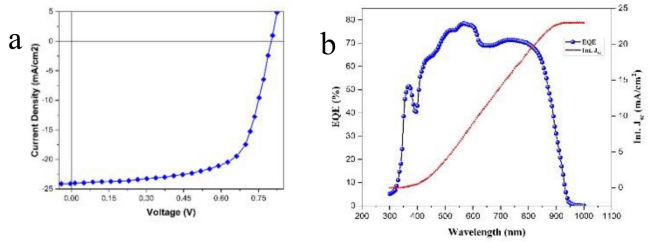

Fig. 3. (a) *J–V* graphs under AM1.5 G, 100 mW/cm^2. (b) EQE of the OSC with integrated J_{SC}.

TABLE I
PHOTOVOLTAIC PARAMETERS OF THE DEVICE UNDER THE ILLUMINANCE OF AM1.5 G

J_{SC} (mA/cm^2)	V_{OC} (V)	FF (%)	PCE (%)	R_S (Ω.cm^2)	R_{Sh} (Ω.cm^2)
24.07	0.80	66.81	12.88 (12.45) *	5.32	180.92

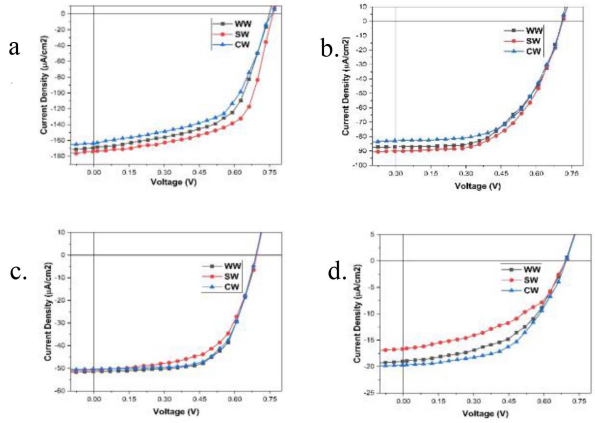

Fig. 4. (a) *J–V* data of devices under different white lights with 1000 lux intensity, (b) white lights with 500 lux intensity, and (c) white lights with 300 lux intensity. (d) *J–V* data of devices under different white lights with 100 lux intensity.

short-circuit current J_{SC} of 24.07 mA/cm^2, open-circuit voltage V_{OC} of 0.80 V, and fill factor (FF) of 66.81%. The external quantum efficiency (EQE) response of the OSC is displayed in Fig. 3(b). The integrated J_{sc} from EQE data is 22.99 mA/cm^2. The devices were then illuminated under white LED, one of the most typical light settings in standard rooms or offices. Here, we have chosen three different kinds of white LEDs for this experiment, namely CW, SW, and WW LED. The significant difference between these three types of LED is that they vary in their CCT values. The CCT refers to how our eyes perceive the light. The CCT values of WW, SW, and CW LED for this experiment are 3000 K, 4000 K, and 6500 K, respectively [26], [27], [39], [40]. For indoor applications, especially personal indoor places, such as a dining hall, kitchen, or bedroom, people usually set with WW LEDs as it is more "yellowish" when we see them and are often said to be comforting and cosy. People prefer CW LEDs in professional setups, such as offices or even some shops, as it is more "bluish," which helps in productivity. In reality, the actual preference of the light depends on the people's comfort level. But it is to be noted that the white LEDs are still preferred as it does not heat up and produce light, consuming less power [27].

Furthermore, the intensities of the LEDs mentioned above were also varied to study the intensity relation of the OSC with their performance. The choice of intensities varies from person to person and application to application. A "well-lit" room has typical intensities from 500 to 1000 lux, while anything below 100 lux is "dimly lit" or "poorly lit." People prefer intensities around 300 lux for reading and indoor chores. However, the preference varies with the choice and expertise of work. Here, we choose four particular values of intensities, i.e., 1000, 500, 300, and 100 lux. These values were chosen as it has more household applications and are commonly preferred by people [41].

All the *J–V* parameters were recorded (see Fig. 4), and the following sections explain the variation and explanation of different photovoltaic parameters under these circumstances. In this work, we try to understand how the devices work under different kinds of white LEDS with varied intensities and how different photovoltaic parameters play a significant role. Such a study has future implications for applying OSCs in the self-sustaining IoTs.

B. *Analysis of the Variation of* V_{OC} *and* J_{SC} *With Intensity*

Open-circuit voltage (V_{OC}) is a deciding parameter of the quality of solar cells. The open-circuit voltage of solar cells directly depends on the energy levels of the active material. The difference between the HOMO level of donor and the LUMO of the acceptor gives the maximum attainable V_{OC}. However, it is observed that there is a decrease in V_{OC} in indoor lighting conditions.

According to the Shockley diode equation, solving for V_{OC} can be expressed as

$$V_{\mathrm{OC}} = \frac{nkT}{q} \ln \frac{J_{\mathrm{ph}}}{J_O}$$

where k is Boltzmann's constant, T is the temperature, n is the ideality factor of the cell, and q is the elementary charge. J_{ph} and J_o are the photocurrents and dark currents, respectively [42], [43], [44].

The photocurrent generated under low-light conditions is less than that compared with 1 sun conditions, as the carrier density is low. This relation is shown in the equation above. At lower light intensities, the recombination increases as comparatively fewer photons are available for charge generation. This increases the trap states and further causes voltage losses. Also, at these levels of intensities, the dark current and leakage currents, which are neglected in the AM1.5 G lighting, become significant [45].

The V_{OC} is 0.80 V for the solar spectrum (AM1.5 G) (see Table I). However, it comes down to 0.75 V, 0.76 V, and 0.76 V, respectively, to WW, SW, and CW LED at 1000 lux (see Table II). Furthermore, when we reduce the intensities to 100 lux, the V_{OC} comes to 0.69 V for all three white LEDs under consideration (see Table V). The percentage change of V_{OC} from AM1.5 G to 100 lux light intensity is 13.75% for the LED lights. It could be

TABLE II
PHOTOVOLTAIC PARAMETERS OF THE DEVICE UNDER 1000 LUX ILLUMINATION OF DIFFERENT LED SOURCES

Light Source	J_{SC} ($\mu A/cm^2$)	V_{OC} (V)	FF (%)	PCE (%)
CW LED	163.56	0.76	56.28	22.03 (21.56) *
SW LED	173.78	0.76	62.32	27.58 (27.34) *
WW LED	169.06	0.75	58.17	24.72 (24.43) *

TABLE III
PHOTOVOLTAIC PARAMETERS OF THE DEVICE UNDER 500 LUX ILLUMINATION OF DIFFERENT LED SOURCES

Light Source	J_{SC} ($\mu A/cm^2$)	V_{OC} (V)	FF (%)	PCE (%)
CW LED	82.84	0.71	56.84	20.99 (20.56) *
SW LED	90.12	0.71	55.21	23.53 (23.21) *
WW LED	87.12	0.71	52.94	22.05 (21.67) *

TABLE IV
PHOTOVOLTAIC PARAMETERS OF THE DEVICE UNDER 300 LUX ILLUMINATION OF DIFFERENT LED SOURCES

Light Source	J_{SC} ($\mu A/cm^2$)	V_{OC} (V)	FF (%)	PCE (%)
CW LED	50.38	0.69	64.35	23.49 (23.12) *
SW LED	50.64	0.69	59.00	22.98 (22.48) *
WW LED	51.41	0.69	63.81	25.43 (25.08) *

TABLE V
PHOTOVOLTAIC PARAMETERS OF THE DEVICE UNDER 100 LUX ILLUMINATION OF DIFFERENT LED SOURCES

Light Source	J_{SC} ($\mu A/cm^2$)	V_{OC} (V)	FF (%)	PCE (%)
CW LED	19.73	0.69	53.83	23.22 (22.76) *
SW LED	16.64	0.69	45.72	17.58 (17.21) *
WW LED	18.99	0.69	50.41	22.18 (22.81) *

assumed from the observation that, as the intensity of the light gets reduced, the open-circuit voltage also gets reduced, owing to fewer photons and more trap states at low-intensity levels. Higher retentivity of voltage (86.25%) for the white LEDs shows that OSCs perform well in low-light conditions.

The J_{SC} (short-circuit current) is the maximum current generated by the solar cells when the terminals are shorted. When the light is incident on the cell's active layer, electron–hole pairs are generated. As the separation occurs, they further drift apart in the opposite directions, contributing to the current generated in the cell. The photons of the light trigger the whole process. The white LED has a limited spectrum (300–800 nm), contributing fewer photons than solar radiation. Furthermore, indoor settings have ambient light conditions that reduce the intensity, restricting more photons and resulting in less current [46].

The *J–V* data provide strong vis-à-vis the above fact, as we observe a significant reduction of current (24.07 mA/cm^2 to $\sim$163 μA/cm^2) from solar radiation to 1000 lux of white LED (see Table II). The J_{SC} shows steep fluctuation as the intensities are varied from 1000 to 100 lux (169.06 μA/cm^2 $\rightarrow$ 18.99 μA/cm^2 in WW, 173.78 μA/cm^2 $\rightarrow$ 16.64 μA/cm^2 in SW, and 163.56 μA/cm^2 $\rightarrow$ 19.73 μA/cm^2 in CW) (see Tables II and V). This sudden depletion of short-circuit current is due to fewer photons available for the photocurrent contributions and the prevalence of recombination over the generation of free carriers. The data correspond to the fact that J_{SC} limits the efficiency of devices in low-light illumination, as the change is drastic.

C. Effect of Parasitic Resistances

The parasitic resistances (R_S and R_{Sh}) are vital in deciding the OSCs' FF under indoor conditions. Series resistances encompass the resistances of the equivalent diode circuit with all the contact resistances. Shunt resistance accounts for the leakage current in the effective circuit. For a device with high FF, we need series resistance to be as low as possible (ideally zero), while shunt resistances are high (ideally infinite)—higher FF results in higher PCE [47], [48].

In the 1 sun conditions, series resistance is a limiting factor that governs the FF of OSC. But at low-light conditions, R_{Sh} plays a pivotal role in deciding the FF (see Tables S1–S4 of the Supplementary Material). At low carrier densities, the recombination becomes prevalent, making the role of R_{Sh} dominant. The series and shunt resistances are calculated and tabulated by fitting with the diode equation given in the supplementary material (see Tables S1–S4).

From the table, it can be observed that there is an increase in FF as the intensities are lower (see Tables II–V). Also, at lower intensities, the series resistances show constant growth. This should contribute to the reduction of FF. Still, as the leakage current is less than that compared with 1 sun condition, there is a significant increase in shunt resistance, which cancels out the increase in the series resistance effect (see Tables S1–S4 of the

Supplementary Material). The net result is an increase in the FF, which is in accordance with the experimental results.

III. Conclusion

In this study, we proposed a systematic approach to how the CCT and intensities of white LED, namely WW, SW, and CW, affect the photovoltaic parameters of the OSC. BHJ OSCs of D18 and Y12 were made in an inverted manner and were illuminated under AM1.5 G and different white LEDs. Furthermore, the intensities of these white LEDs varied, and photovoltaic parameters were calculated and studied.

It is found that the V_{OC} decreases with the intensity of the illuminated light. Among the devices, CW light has the best V_{OC} retention (86.25%). The current (J_{SC}) remained almost the same, with SW showing a bit more average current than its counterparts. Yet, the current has reduced sharply with the decrease in the intensity of the light, which is due to an increase in recombination and the availability of fewer photons for charge generation. The FF showed an increase with the decrease in the illumination intensity. The change in FF is because of parasitic resistances, which play a massive role at lower intensities. Although the series and shunt resistances increased with decreased intensity, a sharp reduction in the leakage current is observed. This increases the shunt resistance considerably compared with series resistances that offer high FF. Among the LEDs, the CW LED showed the best FF.

From the performance of the devices under indoor illumination, we observe that the SW LED initially performs better, but when the intensities are further reduced to as low as 300 lux or 100 lux, CW LEDs show better performance. They show superior FF and PCE at lower light intensities. This is possible due to better spectral matching of the CW LED with the device's active layer. The spectra of CW LED show a sharp peak in the blue region (300–500 nm). We can see a high absorption and conversion of photons in the same area from the device EQE [see Fig. 3(b)]. This is owed to the absorbance of D18.

From these observations, it can be concluded that CW LED is better suited for D18-based indoor OSCs, owing to high spectral matching. Furthermore, CW LED has more "blue color components," as evidenced by the spectra. It also results in more input power, helping to improve photovoltaic parameters. The results prove that a systematic study of the quantity (intensity) and quality (CCT) of light is important for integrating OSCs for IoT. The choice of light setting, along with the selection of materials for the OSC, is vital for the efficient harvest of indoor light for IoTs.

Appendix

"$*$ (asterisk)" in the tables refers to the average value of eight devices.

Acknowledgment

The authors would like to thank The LNM Information Technology, Jaipur, for the peer support, with whom the fruitful discussions have brought the best out of this work.

References

[1] J. Luke, E. J. Yang, C. Labanti, S. Y. Park, and J.-S. Kim, "Key molecular perspectives for high stability in organic photovoltaics," *Nature Rev. Mater.*, vol. 8, no. 12, pp. 839–852, Oct. 2023, doi: 10.1038/s41578-023-00606-5.

[2] J. Yi, G. Zhang, H. Yu, and H. Yan, "Advantages, challenges and molecular design of different material types used in organic solar cells," *Nature Rev. Mater.*, vol. 9, no. 1, pp. 46–62, Dec. 2023, doi: 10.1038/s41578-023-00618-1.

[3] P. Ding, D. Yang, S. Yang, and Z. Ge, "Stability of organic solar cells: Toward commercial applications," *Chem. Soc. Rev.*, vol. 53, no. 5, pp. 2350–2387, 2024, doi: 10.1039/D3CS00492A.

[4] E. Antolin, J. Urieta-Mora, A. Molina-Ontoria, and N. Martín, "Organic solar cells: Principles, materials, and working mechanism," *Curr. Opin. Colloid Interface Sci.*, vol. 76, Apr. 2025, Art. no. 101893, doi: 10.1016/j.cocis.2024.101893.

[5] C. Li et al., "Non-fullerene acceptors with high crystallinity and photoluminescence quantum yield enable >20% efficiency organic solar cells," *Nature Mater.*, vol. 24, no. 3, pp. 433–443, Mar. 2025, doi: 10.1038/s41563-024-02087-5.

[6] H. Chen et al., "Organic solar cells with 20.82% efficiency and high tolerance of active layer thickness through crystallization sequence manipulation," *Nature Mater.*, vol. 24, no. 3, pp. 444–453, Mar. 2025, doi: 10.1038/s41563-024-02062-0.

[7] S. Wang et al., "Achieving 20% efficiency in organic solar cells through conformationally locked solid additives," *Adv. Energy Mater.*, Jan. 2025, Art. no. 2405205, doi: 10.1002/aenm.202405205.

[8] J. Wang et al., "Isomerism effect of 3D dimeric acceptors for non-halogenated solvent-processed organic solar cells with 20% efficiency," *Angewandte Chemie Int. Ed.*, vol. 64, no. 12, Mar. 2025, Art. no. e202423562, doi: 10.1002/anie.202423562.

[9] J. Fu et al., "Rational molecular and device design enables organic solar cells approaching 20% efficiency," *Nature Commun.*, vol. 15, no. 1, Feb. 2024, Art. no. 1830, doi: 10.1038/s41467-024-46022-3.

[10] S. Guan et al., "Self-assembled interlayer enables high-performance organic photovoltaics with power conversion efficiency exceeding 20%," *Adv. Mater.*, vol. 36, no. 25, Jun. 2024, Art. no. e2400342, doi: 10.1002/adma.202400342.

[11] Y. Jiang et al., "Non-fullerene acceptor with asymmetric structure and phenyl-substituted alkyl side chain for 20.2% efficiency organic solar cells," *Nature Energy*, vol. 9, no. 8, pp. 975–986, Jun. 2024, doi: 10.1038/s41560-024-01557-z.

[12] M. A. Alkhalayfeh, A. Abdul Aziz, M. Z. Pakhuruddin, K. M. M. Katubi, and N. Ahmadi, "Recent development of indoor organic photovoltaics," *Physica Status Solidi (a)*, vol. 219, no. 5, Mar. 2022, Art. no. 2100639, doi: 10.1002/pssa.202100639.

[13] M.-Z. Sha, Y.-J. Pu, H. Yin, and X.-T. Hao, "Recent progress of indoor organic photovoltaics—From device performance to multifunctional applications," *Org. Electron.*, vol. 114, Mar. 2023, Art. no. 106736, doi: 10.1016/j.orgel.2022.106736.

[14] X. Liu, S. Xu, B. Tang, and X. Song, "Indoor organic photovoltaics for low-power Internet of Things devices: Recent advances, challenges, and prospects," *Chem. Eng. J.*, vol. 497, Oct. 2024, Art. no. 154944, doi: 10.1016/j.cej.2024.154944.

[15] R. Suthar, H. Dahiya, S. Karak, and G. D. Sharma, "Indoor organic solar cells for low-power IoT devices: Recent progress, challenges, and applications," *J. Mater. Chem. C*, vol. 11, no. 37, pp. 12486–12510, 2023, doi: 10.1039/D3TC02570E.

[16] S. A. Abubaker and M. Z. Pakhuruddin, "Progress and development of organic photovoltaic cells for indoor applications," *Renewable Sustain. Energy Rev.*, vol. 203, Oct. 2024, Art. no. 114738, doi: 10.1016/j.rser.2024.114738.

[17] X. Chen et al., "Indoor photovoltaic materials and devices for self-powered Internet of Things applications," *Mater. Today Energy*, vol. 44, Aug. 2024, Art. no. 101621, doi: 10.1016/j.mtener.2024.101621.

[18] J. Zhu, J. Xia, Y. Li, and Y. Li, "Perspective on flexible organic solar cells for self-powered wearable applications," *ACS Appl. Mater. Interfaces*, vol. 17, no. 4, pp. 5595–5608, Jan. 2025, doi: 10.1021/acsami.4c12238.

[19] M. Jahandar, S. Kim, and D. C. Lim, "Indoor organic photovoltaics for self-sustaining IoT devices: Progress, challenges and practicalization," *ChemSusChem*, vol. 14, no. 17, pp. 3449–3474, Sep. 2021, doi: 10.1002/cssc.202100981.

[20] R. Rajagopalan et al., "Halogenation strategy: Simple wide band gap nonfullerene acceptors with the bodipy-thiophene-backboned polymer donor for enhanced outdoor and indoor photovoltaics," *ACS Appl. Mater. Interfaces*, vol. 16, no. 34, pp. 45265–45274, Aug. 2024, doi: 10.1021/acsami.4c08769.

[21] T. Hyuk Kim, J. Jin Chung, M. Ahsan Saeed, S. Youn Lee, and J. Won Shim, "High-efficiency (over 33%) indoor organic photovoltaics with band-aligned and defect-suppressed interlayers," *Appl. Surf. Sci.*, vol. 610, Feb. 2023, Art. no. 155558, doi: 10.1016/j.apsusc.2022.155558.

[22] W. Wang et al., "High-performance organic photovoltaic cells under indoor lighting enabled by suppressing energetic disorders," *Joule*, vol. 7, no. 5, pp. 1067–1079, May 2023, doi: 10.1016/j.joule.2023.04.003.

[23] W. Wang et al., "Indoor organic photovoltaic module with 30.6 % efficiency for efficient wireless power transfer," *Nano Energy*, vol. 128, Sep. 2024, Art. no. 109893, doi: 10.1016/j.nanoen.2024.109893.

[24] T. Zhang et al., "A medium-bandgap nonfullerene acceptor enabling organic photovoltaic cells with 30% efficiency under indoor artificial light," *Adv. Mater.*, vol. 34, no. 43, Oct. 2022, Art. no. 2207009, doi: 10.1002/adma.202207009.

[25] Q. Wang, H. Xu, F. Zhang, and Z. Wang, "Influence of color temperature on comfort and preference for LED indoor lighting," *Optik (Stuttg)*, vol. 129, pp. 21–29, Jan. 2017, doi: 10.1016/j.ijleo.2016.10.049.

[26] A. Venkateswararao, J. K. W. Ho, S. K. So, S.-W. Liu, and K.-T. Wong, "Device characteristics and material developments of indoor photovoltaic devices," *Mater. Sci. Eng., R, Rep.*, vol. 139, Jan. 2020, Art. no. 100517, doi: 10.1016/j.mser.2019.100517.

[27] B. Zhang et al., "Color-temperature dependence of indoor organic photovoltaic performance," *Org. Electron.*, vol. 104, May 2022, Art. no. 106477, doi: 10.1016/j.orgel.2022.106477.

[28] Y. Lin et al., "Study on the correlations between color rendering indices and the spectral power distribution," *Opt. Exp.*, vol. 22, no. S4, pp. A1029–A1039, Jun. 2014, doi: 10.1364/OE.22.0A1029.

[29] W. B. Tarique and A. Uddin, "A review of progress and challenges in the research developments on organic solar cells," *Mater. Sci. Semicond. Process.*, vol. 163, Aug. 2023, Art. no. 107541, doi: 10.1016/j.mssp.2023.107541.

[30] K. Khandelwal et al., "Unraveling the impact of thickness on active layer morphology and device performance of semitransparent organic solar cells: A comprehensive study," *ACS Appl. Energy Mater.*, vol. 6, no. 19, pp. 10078–10087, Oct. 2023, doi: 10.1021/acsaem.3c01685.

[31] J. Fu et al., "19.31% binary organic solar cell and low non-radiative recombination enabled by non-monotonic intermediate state transition," *Nature Commun.*, vol. 14, no. 1, Mar. 2023, Art. no. 1760, doi: 10.1038/s41467-023-37526-5.

[32] E. Feng et al., "Organic solar cells with D18 or derivatives offer efficiency over 19%," *J. Semicond.*, vol. 45, no. 5, May 2024, Art. no. 050201, doi: 10.1088/1674-4926/45/5/050201.

[33] D. Han and S. Yoo, "The stability of normal vs. inverted organic solar cells under highly damp conditions: Comparison with the same interfacial layers," *Sol. Energy Mater. Sol. Cells*, vol. 128, pp. 41–47, Sep. 2014, doi: 10.1016/j.solmat.2014.04.036.

[34] Z. Liu, "Enhancing the photovoltaic performance with two similar structure polymers as donors by broadening the absorption spectrum and optimizing the molecular arrangement," *Org. Electron.*, vol. 93, Jun. 2021, Art. no. 106153, doi: 10.1016/j.orgel.2021.106153.

[35] X. Ma et al., "Achieving 17.4% efficiency of ternary organic photovoltaics with two well-compatible nonfullerene acceptors for minimizing energy loss," *Adv. Energy Mater.*, vol. 10, no. 31, Aug. 2020, Art. no. 2001404, doi: 10.1002/aenm.202001404.

[36] Y. Sun, J. H. Seo, C. J. Takacs, J. Seifter, and A. J. Heeger, "Inverted polymer solar cells integrated with a low-temperature-annealed sol-gel-derived ZnO film as an electron transport layer," *Adv. Mater.*, vol. 23, no. 14, pp. 1679–1683, Apr. 2011, doi: 10.1002/adma.201004301.

[37] F. Yang et al., "Synthesis of cesium-doped ZnO nanoparticles as an electron extraction layer for efficient PbS colloidal quantum dot solar cells," *J. Mater. Chem. A*, vol. 6, no. 36, pp. 17688–17697, 2018, doi: 10.1039/C8TA05946B.

[38] H. Hou et al., "Undoped MoOX with oxygen-rich vacancies as hole transport material for efficient indoor/outdoor organic solar cells," *Nano Energy*, vol. 131, Dec. 2024, Art. no. 110173, doi: 10.1016/j.nanoen.2024.110173.

[39] M. C. Scharber and N. S. Sariciftci, "Efficiency of bulk-heterojunction organic solar cells," *Prog. Polym. Sci.*, vol. 38, no. 12, pp. 1929–1940, Dec. 2013, doi: 10.1016/j.progpolymsci.2013.05.001.

[40] K. S. Srivishnu, M. N. Rajesh, S. Prasanthkumar, and L. Giribabu, "Photovoltaics for indoor applications: Progress, challenges and perspectives," *Sol. Energy*, vol. 264, Nov. 2023, Art. no. 112057, doi: 10.1016/j.solener.2023.112057.

[41] S. K. Bhandary, R. Dhakal, V. Sanghavi, and P. K. Verkicharla, "Ambient light level varies with different locations and environmental conditions: Potential to impact myopia," *PLoS One*, vol. 16, no. 7, Jul. 2021, Art. no. e0254027, doi: 10.1371/journal.pone.0254027.

[42] S. Zeiske, W. Li, P. Meredith, A. Armin, and O. J. Sandberg, "Light intensity dependence of the photocurrent in organic photovoltaic devices," *Cell Rep. Phys. Sci.*, vol. 3, no. 10, Oct. 2022, Art. no. 101096, doi: 10.1016/j.xcrp.2022.101096.

[43] C. Labanti et al., "Light-intensity-dependent photoresponse time of organic photodetectors and its molecular origin," *Nature Commun.*, vol. 13, no. 1, Jun. 2022, Art. no. 3745, doi: 10.1038/s41467-022-31367-4.

[44] D. Lübke, P. Hartnagel, M. Hülsbeck, and T. Kirchartz, "Understanding the thickness and light-intensity dependent performance of green-solvent processed organic solar cells," *ACS Mater. Au*, vol. 3, no. 3, pp. 215–230, May 2023, doi: 10.1021/acsmaterialsau.2c00070.

[45] S. Hwang and T. Yasuda, "Indoor photovoltaic energy harvesting based on semiconducting π-conjugated polymers and oligomeric materials toward future IoT applications," *Polym. J.*, vol. 55, no. 4, pp. 297–316, Apr. 2023, doi: 10.1038/s41428-022-00727-8.

[46] P. Hartnagel and T. Kirchartz, "Understanding the light-intensity dependence of the short-circuit current of organic solar cells," *Adv. Theory Simul.*, vol. 3, no. 10, Oct. 2020, Art. no. 2000116, doi: 10.1002/adts.202000116.

[47] B. Qi and J. Wang, "Fill factor in organic solar cells," *Phys. Chem. Chem. Phys.*, vol. 15, no. 23, pp. 8972–8982, 2013, doi: 10.1039/c3cp51383a.

[48] E. E. van Dyk and E. L. Meyer, "Analysis of the effect of parasitic resistances on the performance of photovoltaic modules," *Renewable Energy*, vol. 29, no. 3, pp. 333–344, Mar. 2004, doi: 10.1016/S0960-1481(03)00250-7.